Lossless Scalar Metasurfaces for Anomalous Reflection Based on Efficient Surface Field Optimization

Do-Hoon Kwon, *Senior Member, IEEE*

***Abstract*—For polarization-preserving anomalous plane-wave reflections by impenetrable surfaces, an efficient numerical field optimization technique is presented for designing lossless metasurfaces. Auxiliary surface waves copolarized with the incident and reflected plane waves are introduced and optimized such that the scalar surface impedance characterizing the reflecting surface approach a purely reactive profile. The resulting inhomogeneous scalar reactance can be discretized for realization as a periodic metasurface. Full-wave simulation of a physical design that is directly translated from the optimized reactance profile shows near-perfect anomalous reflection.**

***Index Terms*—Electromagnetic reflection, metasurfaces, periodic structures, surface waves (SWs).**

I. Introduction

RECENT development of electromagnetic metasurfaces, a two-dimensional equivalent of volumetric metamaterials [1], has witnessed emergence of new theory and applications for a host of novel wave manipulation functions from microwave to optical regimes. In particular, gradient metasurfaces [2] and Huygens' metasurfaces [3] have emerged as key enablers for wavefront transformations with high efficiencies for both reflective and transmissive applications [3]–[6].

For anomalous reflectors based on the generalized reflection law [7], it has been revealed that the power efficiency into the anomalous direction significantly deteriorates for large deflection angles [8], [9]. If the sum of the incident and reflected waves is specified to be the total fields, the resulting reflecting surface is found to exhibit alternating active and lossy spatial ranges while remaining power-neutral on average. Introducing surface waves (SWs) can lead to pointwise lossless surface properties. For Ω-bianisotropic metasurfaces, adding auxiliary evanescent waves to the propagating waves (PWs) and enforcing a local power conservation relation produced passive and lossless surface specifications for perfect anomalous reflection and beam splitting [10], [11]. In [12], a printed reactive surface design based on the leaky-wave antenna principle was numerically optimized, and a power efficiency of 94% was experimentally demonstrated for a 0°-to-70° reflector. Most recently, the concept of metagratings [13], [14] has been introduced, where only one or two inclusions per period are optimized to provide anomalous reflection control. An analytical design method for printed metagratings for anomalous reflection has been reported in [15].

In this letter, lossless metasurfaces characterized by a scalar surface impedance are designed for perfect anomalous reflection based on field optimization. A set of copolarized SWs are introduced and the total tangential fields are optimized such that the net power density normal to the surface is *minimized everywhere* toward obtaining a purely reactive surface impedance. The SWs are the evanescent Floquet waves of infinite periodic structures as those in [11] and [14]. Here, multiple evanescent modes are introduced and quantitatively controlled. The required nonlinear optimization can be performed efficiently. An example 0°-to-70° reflector at 6 GHz in the transverse electric (TE) polarization its designed, and a physical printed metasurface design based on its discretized surface impedance is analyzed.

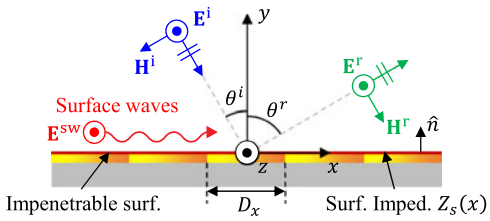

Fig. 1. Anomalous plane-wave reflection in the TE polarization by an impenetrable planar metasurface in the xz plane characterized by a surface impedance Z_s. The SWs are copolarized with the plane waves. The periodic metasurface has a period D_x.

II. Anomalous Reflection With Copolarized SWs

A polarization-preserving anomalous reflection of a plane wave is illustrated in Fig. 1, where the TE (to y) polarization has been chosen. An incident plane wave with fields $(\mathbf{E}^{\mathrm{i}}, \mathbf{H}^{\mathrm{i}})$ illuminates a reflector surface in the xz plane with an incidence angle θ^{i}. All the incident power is reflected into an anomalous reflection angle θ^{r} as a plane wave with fields $(\mathbf{E}^{\mathrm{r}}, \mathbf{H}^{\mathrm{r}})$. With an $e^{j\omega t}$ time convention assumed and suppressed, the incident and reflected E-field vectors are written as

$$\mathbf{E}^{\mathrm{i}} = \hat{z} E_0^{\mathrm{i}} e^{-jk(x \sin\theta^{\mathrm{i}} - y\cos\theta^{\mathrm{i}})}$$
$$\mathbf{E}^{\mathrm{r}} = \hat{z} E_0^{\mathrm{r}} e^{-jk(x \sin\theta^{\mathrm{r}} + y\cos\theta^{\mathrm{r}})} \quad (1)$$

Manuscript received April 2, 2018; revised May 6, 2018; accepted May 10, 2018. Date of publication May 14, 2018; date of current version July 4, 2018.

The author is with the Department of Electrical and Computer Engineering, University of Massachusetts Amherst, Amherst, MA 01003 USA (e-mail: dhkwon@umass.edu).

Digital Object Identifier 10.1109/LAWP.2018.2836299

where $E_0^{\rm i}$ and $E_0^{\rm r}$ are the E-field amplitudes for the incident and reflected plane waves, respectively, and $k = 2\pi/\lambda$ ($\lambda =$ free-space wavelength) represents the free-space wavenumber. It is desired that this reflection function be realized using a pointwise lossless planar metasurface in the xz plane. In a periodic metasurface design, the period D_x of a supercell is set to $D_x = \lambda/|\sin\theta^{\rm r} - \sin\theta^{\rm i}|$.

If no fields other than the incident and reflected plane wave fields are allowed to be present in $y \geq 0$, the resulting metasurface exhibits alternating x-ranges of power loss and gain [8], [9], manifested by positive and negative values for the resistance part R_s of the surface impedance $Z_s = R_s + jX_s$. An evanescent auxiliary field may be introduced without affecting the reflection property of the surface in the far zone, as was done in [11]. The local power conservation principle for obtaining lossless surface parameters in [10] was extended to an impenetrable surface characterized by a tensor surface impedance [16]. However, accurate realization of an inhomogeneous tensor surface impedance is challenging.

Hence, we seek to design a lossless reflector metasurface by introducing SWs that are also TE-polarized like the PWs, as illustrated in Fig. 1. Introducing a finite number of Floquet mode fields, let the tangential E- and H-field components of the total fields on the *surface* be written as

$$E_{tz} = \sum_{n=0}^{N} E_n e^{-j\beta_n x} \qquad H_{tx} = \sum_{n=0}^{N} H_n e^{-j\beta_n x} \tag{2}$$

where n is the Floquet mode index, $\beta_n = k\sin\theta^{\rm i} + 2n\pi/D_x$ is the associated x-wavenumber, and E_n and H_n are the mode field amplitudes. For zero specular reflection and complete power-preserved reflection into the $n = 1$ harmonic, we set

$$E_n = \begin{cases} E_0^{\rm i}, & n = 0 \\ E_0^{\rm r}, & n = 1 \end{cases} \qquad H_n = \begin{cases} -E_0^{\rm i}\cos\theta^{\rm i}/\eta, & n = 0 \\ E_0^{\rm r}\cos\theta^{\rm r}/\eta, & n = 1 \end{cases} \tag{3}$$

together with

$$|E_0^{\rm r}| = |E_0^{\rm i}|\sqrt{\frac{\cos\theta^{\rm i}}{\cos\theta^{\rm r}}} \tag{4}$$

where $\eta \approx 377\ \Omega$ is the free-space intrinsic impedance. All the remaining coefficients E_n $(n = 2, \ldots, N)$ are the complex amplitudes of the SWs to be determined. The H-field amplitudes are related to the E-field amplitudes via $H_n = -j\alpha_n E_n/\eta$, where $\alpha_n = \sqrt{\beta_n^2 - k^2}$ is the attenuation constant of the nth Floquet harmonic in the y-axis direction.

For a normal incidence that will be considered ($\theta^{\rm i} = 0$), the $n = 2$ harmonic becomes evanescent when $\theta^{\rm r} > 30^\circ$. This is the most applicable scenario for large-angle deflections in the proposed design approach, as the power reflection efficiency into moderate deflection angles ($\theta^{\rm r} < 30^\circ$) based on the generalized reflection law is already high [12]. In (3), setting $E_0 = E_0^{\rm i}$ is equivalent to enforcing zero specular reflection; the absence of an $n = -1$ term in (2) implies no reflection into the $-\theta^{\rm r}$ direction.

The impenetrable metasurface is characterized by an inhomogeneous scalar surface impedance defined by

$$Z_s(x) = R_s(x) + jX_s(x) = -\frac{E_{tz}}{H_{tx}}. \tag{5}$$

III. Surface Field Optimization for a Lossless Surface

At any given point on the surface, a locally lossless property is associated with a purely imaginary value for Z_s. Considering that $R_s = -\operatorname{Re}\{E_{tz}/H_{tx}\} = -\operatorname{Re}\{E_{tz}H_{tx}^*\}/|H_{tx}|^2$, the no-loss condition is equivalent to the normal component of the Poynting vector satisfying

$$S_y(x) = \frac{1}{2}\operatorname{Re}\{E_{tz}H_{tx}^*\} = 0. \tag{6}$$

Serving as the design principle, (6) is the local power conservation relation [10] applicable to an impenetrable scalar metasurface. Using (2), the Poynting vector component is expressed as

$$S_y = \frac{1}{2}\sum_{p=0}^{N}\left[|C_p^+|\cos(\beta_p x + \phi_p^+) + |C_p^-|\cos(\beta_p x - \phi_p^-)\right] \tag{7}$$

where $|C_p^\pm|$ and $\phi_p^\pm$ are the magnitude and phase of

$$C_p^+ = \sum_{q=p}^{N} E_{q-p}H_q^* \qquad C_p^- = \sum_{q=0}^{N-p} E_{q+p}H_q^* \tag{8}$$

respectively. There are $N+1$ cosine harmonics in (7) in general, but the constant ($p = 0$) term vanishes owing to (4). We have an $N-1$ number of SW E-field amplitudes, E_n $(n = 2, \ldots, N)$, for control. Furthermore, $C_p^\pm$ are nonlinear functions of E_n. Hence, it is unlikely that exact solutions for E_n's to (6) exist. Still, approximate solutions can be sought by minimizing a properly defined error function for S_y. One reasonable choice is the sum of squared magnitudes of the cosine harmonics in (7)

$$e_{\rm sq} = \sum_{p=0}^{N}\left[\left(\operatorname{Re}\{C_p^+ + C_p^-\}\right)^2 + \left(\operatorname{Im}\{C_p^+ - C_p^-\}\right)^2\right]. \tag{9}$$

The $N-1$ number of SW amplitudes can be optimized to minimize $e_{\rm sq}$. While nonlinear, this is an algebraic optimization, which may be performed efficiently. In this letter, the *fminsearch* function in MATLAB has been used. Once the optimized SW fields are determined, Z_s is evaluated using (5). If $R_s \approx 0$ is validated for all x, the resistance part can be discarded to define a reactive surface impedance as

$$Z_s^{\rm reac}(x) = jX_s(x) \tag{10}$$

which represents a pointwise lossless scalar impedance surface.

IV. Design Example

An example 0°-to-70° ($\theta^{\rm i} = 0, \theta^{\rm r} = 70^\circ$) anomalous plane-wave reflector is designed as a periodic metasurface with a period $D_x = 1.064\ \lambda$. For a unit-amplitude incident E-field ($E_0^{\rm i} = 1$ V/m), the reflected E-field magnitude becomes larger than unity due to power conservation. It was observed that the minimized $e_{\rm sq}$ monotonically decreased with an increasing choice for N. This agrees with the anticipation that a larger

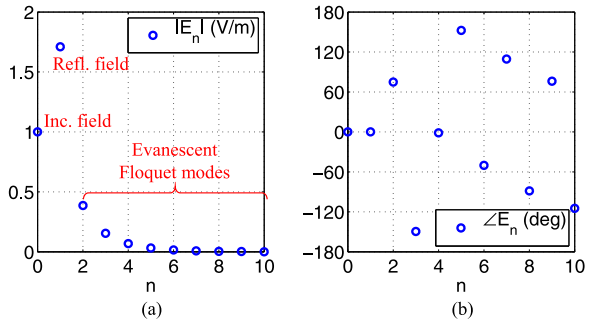

Fig. 2. Floquet mode coefficients of the optimized total fields. (a) Magnitude. (b) Phase of the optimized E-field coefficients.

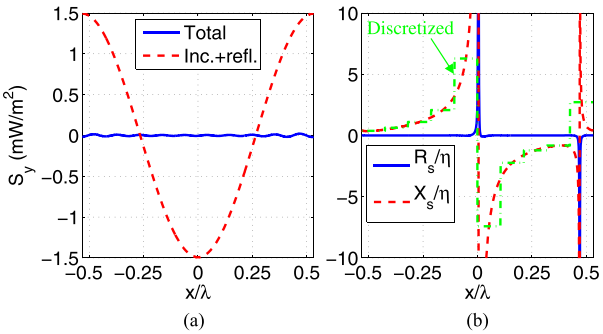

Fig. 3. Characteristics of the optimized design. (a) Power density normal to the metasurface. (b) Retrieved surface impedance Z_s normalized by η.

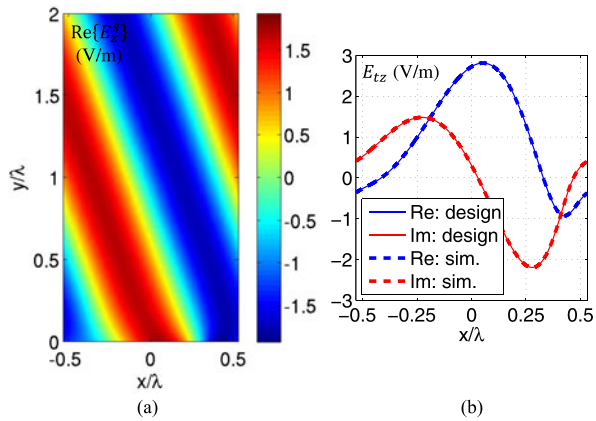

Fig. 4. Reflection properties of the metasurface represented by an inhomogeneous reactive surface impedance $Z_s^{\text{reac}}(x)$. (a) Snapshot of the scattered E-field distribution. (b) Comparison of the total tangential E-field at $y = 0$.

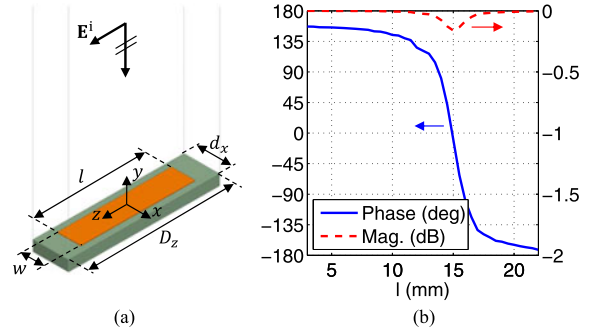

Fig. 5. Unit cell for a printed metasurface realization. (a) Unit cell of a thin copper strip of length l and width w printed on a grounded dielectric substrate. The cell dimensions in the xz plane are $d_x \times D_z$. (b) Plane-wave reflection coefficient with respect to l at 6 GHz.

degree of design freedom would be able to satisfy (6) more closely. It is recognized that an arbitrary reflection phase is available with respect to the phase reference x-coordinate. As a result, a particular target reflection phase does not impact the process or result of the design, except for an appropriate shift of the coordinate origin. Arbitrarily selecting a zero phase angle, we set $E_0^{\text{r}} = 1.71$ V/m. A set of nine $(N = 10)$ SW E-field amplitudes, E_n $(n = 2, \ldots, 10)$, is optimized for minimizing the error, reaching $e_{\text{sq}} = 5.66 \times 10^{-5}$ relative to the value associated with a null SW.

The E-field coefficients E_n of the optimized fields are plotted with respect to the mode index n in Fig. 2. It is found that $|E_n|$ $(n = 2, \ldots, 10)$ continuously decreases with an increasing n, as β_n moves deeper into the evanescent spectral range. The phase angles nearly span a complete 360° range. Over one period, the Poynting vector component normal to the surface is compared in Fig. 3(a) between the optimized total fields and the PWs only. As expected, the power density associated with the incident and reflected waves only alternates between active and lossy ranges with a zero overall average. While (6) is not exactly satisfied at every x, $S_y(x)$ varies and remains close to zero over the entire period. The surface impedance $Z_s(x)$ associated with the optimized fields is shown in Fig. 3(b). The resistance $R_s(x)$ stays near zero over the period except around two isolated points at $x \approx 0.004\ \lambda, 0.47\ \lambda$. It turns out that $H_{tx} \approx 0$ (and thus $S_y \approx 0$) at these points, leading to a diverging behavior for both R_s and X_s. Therefore, setting $R_s = 0$ for all x, including around the two narrow ranges, is not expected to perturb the expected field distributions noticeably. Although X_s diverges to $\pm\infty$ at isolated locations, it does not cross zero. The corresponding reflection phase span for normal incidence is found to be 243.2°, with the phase ranging from −101.8° to 141.4°.

Reflection performance of the lossless metasurface, characterized by the continuously varying impedance $Z_s^{\text{reac}}(x)$ enforced on the surface at $y = 0$, is analyzed using COMSOL Multiphysics. Fig. 4(a) plots a snapshot of the scattered E-field distribution. The presence of the SWs is visible only near the metasurface. Slightly away from $y = 0$, a pure plane wave propagating in the +70° direction with a correct magnitude of 1.71 V/m is established. Simulation results show that 100% of the power is reflected into the anomalous direction. In Fig. 4(b), $E_{tz}(x)$ is compared over a period between the design [(2) with the E-field amplitudes from Fig. 2] and simulation. An excellent agreement is observed, signifying that the metasurface designed using the optimized SWs generates the intended field distribution even with the approximation $R_s = 0$.

The lossless metasurface may be realized as a periodic printed reactive surface aimed at synthesizing a discretized version of $Z_s^{\text{reac}}(x)$ at a subwavelength interval. We choose an array of thin conductor strips printed on a grounded dielectric substrate at a design frequency of 6 GHz $(\lambda = 5\,\text{cm})$. The unit cell is illustrated in Fig. 5(a) together with an incident plane wave for reflection coefficient evaluation. The fixed geometrical parameters are given by $d_x = D_x/10 = 5.32$, $D_z = 0.45\ \lambda = 22.5$, and $w = 3.5$ (all in mil-

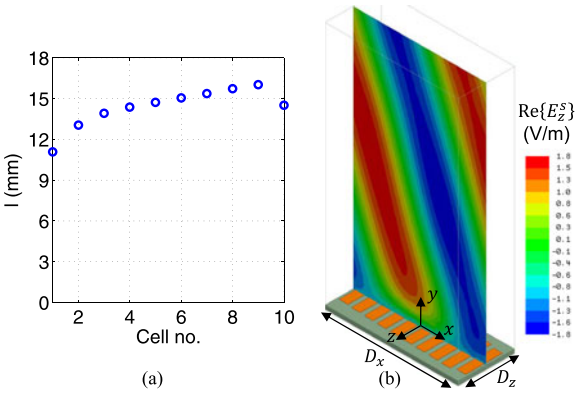

Fig. 6. Physical design and simulated performance of a printed metasurface. (a) Length distribution of copper strips in a supercell. (b) Snapshot of the scattered E-field distribution obtained using HFSS.

limeters). The dielectric substrate is Rogers RT/duroid 5880 (with a relative permittivity $\epsilon_r = 2.2$ and a loss tangent $\tan\delta = 0.0009$) of thickness 1.575 mm. The thickness of the copper strip is 70 μm. Using a z-polarized plane wave at normal incidence, the unit cell was simulated under periodic boundary conditions for the complex reflection coefficient referenced in the plane of the strip ($z = 0$) using Ansys HFSS. The plane-wave reflection coefficient is plotted in Fig. 5(b) with respect to l. Over $3\,\text{mm} < l < 22\,\text{mm}$, the reflection phase ranges from -171.9° to 156.9°, which includes the required phase range associated with Z_s^{reac} for the design. The strip becomes resonant near $l = 15\,\text{mm}$, where the return loss due to conductor and dielectric losses reaches a maximum value of 0.16 dB.

Next, a supercell is designed by cascading 10 unit cells. Based on the local periodicity approach, the length of each strip is read from the reflection phase curve in Fig. 5(b) using the discretized surface reactance shown in Fig. 3(b) as a green dash-dot curve. The lengths of the copper strips in a supercell are shown in Fig. 6(a), ranging from 11.1 to 16.0 mm. Under periodic boundary conditions, reflection from the physical metasurface was simulated using HFSS, and a snapshot of the scattered E-field distribution in the xy plane is plotted in Fig. 6(b) over $|x| < D_x/2$, $0 < y < 2\,\lambda$ above the supercell geometry. The field near the physical metasurface in Fig. 6(b) is different from that over a mathematically characterized metasurface in Fig. 4(a). However, once removed from the immediate neighborhood of the surface, a pure plane wave is established above the physical metasurface. The HFSS results show that 95.5% of the incident power is reflected into the $+70^\circ$ direction. The powers reflected into the -70° and 0° directions are predicted to be 0.57% and 0.02%, respectively. The remaining 3.9% of the incident power is absorbed by the metasurface.

In [12], the physical metasurface was designed in a single-stage full-wave optimization on the supercell level. In comparison, the design in this letter comprises two stages, where an efficient surface impedance synthesis is followed by individual cell designs assuming local periodicity. Not requiring supercell-level full-wave optimizations for impedance synthesis makes the overall design process efficient. This advantage stems from working with the tangential fields on the surface.

V. Conclusion

For anomalous plane-wave reflection by a planar impenetrable metasurface, a field optimization technique has been presented for designing locally and globally lossless scalar metasurfaces. For a physical design at a microwave frequency, a periodic printed metasurface comprising an array of conductor strips on a grounded dielectric substrate was synthesized. Full-wave simulation of the physical metasurface design predicted near-perfect anomalous reflection in the presence of realistic losses and without a need for supercell-level full-wave optimizations. At an increased complexity in design and realization, the field optimization technique quantifies and controls the behavior of local evanescent fields compared with the recent metagrating reflectors.

References

[1] C. L. Holloway, E. F. Kuester, J. A. Gordon, J. O'Hara, J. Booth, and D. R. Smith, "An overview of the theory and applications of metasurfaces: The two-dimensional equivalents of metamaterials," *IEEE Antennas Propag. Mag.*, vol. 54, no. 2, pp. 10–35, Apr. 2012.

[2] D. Lin, P. Fan, E. Hasman, and M. L. Brongersma, "Dielectric gradient metasurface optical elements," *Science*, vol. 345, pp. 298–302, 2014.

[3] C. Pfeiffer and A. Grbic, "Metamaterial Huygens' surfaces: Tailoring wave fronts with reflectionless sheets," *Phys. Rev. Lett.*, vol. 110, pp. 197 401-1–197 401-5, 2013.

[4] A. Pors, M. G. Nielsen, R. L. Eriksen, and S. I. Bozhevolnyi, "Broadband focusing flat mirrors based on plasmonic gradient metasurfaces," *Nano Lett.*, vol. 13, pp. 829–834, 2013.

[5] X. Ni, A. V. Kildishev, and V. M. Shalaev, "Metasurface holograms for visible light," *Nature Commun.*, vol. 4, pp. 2807-1–2807-6, 2013.

[6] C. Pfeiffer and A. Grbic, "Millimeter-wave transmitarrays for wavefront and polarization control," *IEEE Trans. Microw. Theory Techn.*, vol. 61, no. 12, pp. 4407–4417, Dec. 2013.

[7] N. Yu *et al.*, "Light propagation with phase discontinuities: Generalized laws of reflection and refraction," *Science*, vol. 334, pp. 333–337, Oct. 2011.

[8] N. Mohammadi Estakhri and A. Alù, "Wave-front transformation with gradient metasurfaces," *Phys. Rev. X*, vol. 6, pp. 041 008-1–041 008-17, 2016.

[9] V. S. Asadchy, M. Albooyeh, S. N. Tcvetkova, A. Díaz-Rubio, Y. Ra'di, and S. A. Tretyakov, "Perfect control of reflection and refraction using spatially dispersive metasurfaces," *Phys. Rev. B*, vol. 94, pp. 075 142-1–075 142-14, 2016.

[10] A. Epstein and G. V. Eleftheriades, "Arbitrary power-conserving field transformations with passive lossless Omega-type bianisotropic metasurfaces," *IEEE Trans. Antennas Propag.*, vol. 64, no. 9, pp. 3880–3895, Sep. 2016.

[11] A. Epstein and G. V. Eleftheriades, "Synthesis of passive lossless metasurfaces using auxiliary fields for reflectionless beam splitting and perfect reflection," *Phys. Rev. Lett.*, vol. 117, pp. 256 103-1–256 103-6, 2016.

[12] A. Díaz-Rubio, V. S. Asadchy, A. Elsakka, and S. A. Tretyakov, "From the generalized reflection law to the realization of perfect anomalous reflectors," *Sci. Adv.*, vol. 3, pp. e1 602 714-1–e1 602 714-10, 2017.

[13] Y. Ra'di, D. L. Sounas, and A. Alù, "Metagratings: Beyond the limits of graded metasurfaces for wave front control," *Phys. Rev. Lett.*, vol. 119, pp. 067 404-1–067 404-6, 2017.

[14] A. M. H. Wong and G. V. Eleftheriades, "Perfect anomalous reflection with a bipartite Huygens' metasurface," *Phys. Rev. X*, vol. 8, pp. 011 036-1–011 036-8, 2018.

[15] O. Rabinovich and A. Epstein, "Analytical design of printed-circuit-board (PCB) metagratings for perfect anomalous reflection," Jan. 2018. [Online]. Available: https://arxiv.org/abs/1801.04521

[16] D.-H. Kwon and S. A. Tretyakov, "Perfect reflection control for impenetrable surfaces using surface waves of orthogonal polarization," *Phys. Rev. B*, vol. 96, pp. 085 438-1–085 438-10, 2017.